



Removal of methyl violet 2-B from aqueous solutions using untreated and magnetite-impregnated almond shell as adsorbents

Khalid Saeed^{a,b,*}, Mohammad Ishaq^a, Siraj Sultan^a, Imtiaz Ahmad^a

^a*Institute of Chemical Sciences, University of Peshawar, Khyber Pakhtunkhwa, Pakistan, email: Khalidkhalil2002@yahoo.com (K. Saeed)*

^b*Department of Chemistry, University of Malakand, Khyber Pakhtunkhwa, Pakistan*

Received 3 July 2014; Accepted 31 May 2015

ABSTRACT

The magnetite-impregnated almond shell (MIAS) and untreated almond shell (UAS) were used as adsorbents for the removal of methyl violet 2B from aqueous solution. The adsorption of MV2B from water onto adsorbent surface was investigated in batch adsorption experiments to evaluate the effect of pH, contact time, adsorbent dose, initial dye concentration, and temperature, after being analyzed the surface morphology and elemental composition of the adsorbents. The adsorptions of MV2B onto both adsorbents were favorable in basic medium. The pseudo-second order represents the kinetic adsorption of MV2B on to both adsorbents. Equilibrium isotherm data were analyzed by Langmuir and Freundlich adsorption isotherms, which were best fitted to Langmuir adsorption isotherm model. The monolayer Langmuir adsorption capacities of UAS and MIAS were 29.4 and 33 mg/g, respectively. The thermodynamic parameters including entropy (ΔS), enthalpy (ΔH), and Gibbs free energy (ΔG) indicated that the adsorption of MV2B on to both adsorbents was spontaneous, feasible, and endothermic.

Keywords: Methyl violet 2B; Almond shell; Adsorption; SEM; EDX

1. Introduction

Due to the commercial application of dyes and coloring material, they are being used by almost each industry. Dyes containing wastewater are one of the most important toxic concerns. This is due to the huge consumption of dyes for different purposes, such as dermatological agent, veterinary medicine, and biological stain [1,2]. It has been estimated that approximately 1 million kg/year of dyes are released into river and ocean by textile industry [3]. Different dyes are discharged into the aquatic system from various

industries such as paint, textile, painting, paper, and pulp [1–5]. The toxicity of dyes is because of its permanent color in the water, which has a drastic effect on the animals' skin and eyes [2]. In addition, dyes present in water caused mutagenic, carcinogenic and genotoxic disorder in the human being, animal, and microorganism [6]. The discharge of wastewater containing dyes from various industries not only distorts the beauty of river but also reduces sunlight penetration through water, which affect the photosynthetic potential of aquatic green plants [7]. Dyes are further classified into cationic, anionic, and neutral dye in nature. Among these, cationic dyes are considered to be the most toxic one. Its toxic nature is

*Corresponding author.

due to its maximum solubility in water [5]. Facing these problems, many techniques have been used to treat the dye-contaminated water before discharged into river. Among these methods, ultra-filtration, reverse osmosis, chemical oxidation, ion-exchange membrane filtration, ozone treatment, and adsorption are extensively applied [8,9]. Adsorption is the most attractive technique for the treatment of wastewater polluted by dyes as compared to other techniques, especially in the case when low-cost and easily available adsorbents are used [10,11]. Consequently, many researchers reported the feasibility of economical adsorbents for the treatment of wastewater polluted by dyes and heavy metals. Some of the low-cost adsorbents such as peanut hull [12], rice husk [13], maize cob [14], silica gel [15], alumina [16], almond shell [17,18], tea waste [19], pomegranate shell powder [20], activated carbon [21–23], and saw dust [24] are extensively reported for wastewater treatment.

In this work, almond shell powder was used as a low-cost adsorbent to check its adsorption capacity toward MV2B from aqueous medium. Almond shell powder will be further used as untreated and magnetite-impregnated adsorbents. The main focus of this study was to investigate the adsorption efficiency of the prepared adsorbents from aqueous solution. The effects of various parameters such as pH, contact time, adsorbent dose, initial dye concentration, and temperature on the adsorption of MV2B were also studied. The obtained equilibrium isotherm data were analyzed by Langmuir and Freundlich adsorption isotherms.

2. Experimental

2.1. Materials

MV2B was purchased from Merck Company and used without any further purification. The almond shells were collected from the Board Bazar, Peshawar, Pakistan. The shells were grinded into powder and then sieved through a screener having 120 mesh sizes. The sieved almond shells were then washed with distilled water in order to remove dust particles inherent in almond shell. The shell was then dried and stored for further experimental studies.

2.2. Synthesis of magnetite-impregnated almond shells

Eighty milliliters of double-distilled water, and $\text{FeCl}_2 \cdot 4\text{H}_2\text{O}$ and $\text{FeCl}_3 \cdot 6\text{H}_2\text{O}$ (ratio of 1:2) were taken in flask and heated at 85°C for 30 min. Then, a 20 mL ammonium solution (30%) was added to the mixture solutions, which immediately changed the orange

color of solution into black. At this stage, 6 g of the pretreated almond shell was added to the mixture and heated at 85°C for 2 h and stirred constantly. After 2 h, the magnetite-impregnated almond shell was filtered and washed repeatedly with distilled water in order to remove extra chloride ions. The MIAS was dried in oven and stored for further use.

2.3. Zeta potential of adsorbents before and after adsorption of Methyl Violet 2B dye

The zero point charge (pH_{ZPC}) of both adsorbents before and after adsorption was measured by the following batch equilibrium experiment: 10 mg of each adsorbent before and after adsorption was taken in 10 mL of 0.1 M sodium chloride (NaCl) solution. The initial pH (pH_i) values of the NaCl solutions were adjusted from 1 to 11 with 0.1 M NaOH and HNO_3 solutions. The mixture was equilibrated at 20°C for 24 h and then filtered through Whatman filter paper before measuring the equilibrium pH. The zeta potential of each adsorbent in the equilibrium solutions was measured using Zeta potential analyzer. The value of pH_{ZPC} is the point where the curve of $(\text{pH}_i - \text{pH}_f)$ vs. pH_i crosses the line equal to zero.

2.4. Batch adsorption program

Adsorption of MV2B onto UAS and MIAS was conducted at various adsorption parameters such as different solutions pH, contact time, adsorbent dose, initial dye concentration, and different adsorption temperature. For each experimental study, known volume, initial dye concentration, pH of the MV2B solutions, and known mass of the adsorbent were taken and shacked on shaker for the respective time. The pH of the solutions was adjusted using dilute HCl and NaOH solutions. After the respective adsorption time, the adsorbents were separated from MV2B solution via centrifugation. The dye concentration before and after adsorption from aqueous solution was determined using UV–visible spectrophotometer. The dye adsorbed per unit mass of the adsorbent (mg/g) and the percentage adsorption were calculated using the following equations:

$$q_e = \frac{(C_i - C_e)V}{W} \quad (1)$$

$$R\% = \frac{(C_i - C_e)}{C_i} \times 100 \quad (2)$$

where q_e is the adsorption capacity (mg/g), C_i is the initial concentration of MV2B in aqueous solutions

(mg/L), C_e is the equilibrium concentration of MV2B in aqueous solutions, V is the volume of solutions in liter, and W is the mass of adsorbent in gram.

2.5. Instrumentation

The morphological study of gold-coated was carried out by JEOL, JSM-5910 SEM. The X ray spectrometry (EDX) spectrometric analyses of both adsorbents were performed on EDX (Model INCA 200/Oxford Instruments), in order MIAS and UAS to investigate the elemental composition of the samples. The FT-IR study of MIAS and UAS was performed by Shimadzu IR Prestige-2. The photodegradation study of MV2B was performed using UV–visible spectrophotometer (Shimadzu Module 160-A).

3. Results and discussions

3.1. Surface morphological study of the prepared adsorbents

The SEM analyses were performed in order to study the surface morphologies of prepared adsorbents. It was reported that the adsorbent with porous and rough morphology shows high adsorption capacity [25]. The SEM of dye-loaded adsorbents was also carried out in order to investigate the adsorption of

dyes on each adsorbent from the surface morphological changes. Fig. 1(a–d) shows the SEM images of UAS and MIAS. It can be seen clearly from the Fig. 1(a) and (b) that the morphology of UAS and MIAS is completely different from each other. The surface of the MIAS is more rough and porous than UAS. Thus, from their surface morphology comparison, it can be concluded that the MIAS will have high adsorption capacity than UAS because of its porous and rough surface. Fig. 1(c) and (d) shows the SEM images of UAS and MIAS after the adsorption of MV2B, which clearly shows that the surface of UAS and MIAS is covered by layer of dyes.

3.2. X ray spectrometry (EDX) analysis of the prepared adsorbents

Energy dispersive EDX technique is used for the determination of elemental compositions of the adsorbent. EDX analyses of the prepared adsorbents were carried out in order to determine its elemental compositions. Fig. 2(a) and (b) shows the EDX spectra and quantitative elemental composition of the UAS and MIAS. The EDX spectra of UAS show the highest percentage of carbon and oxygen along with minute quantity of silicon, potassium, and calcium. The EDX spectrum of MIAS shows the highest percentage of

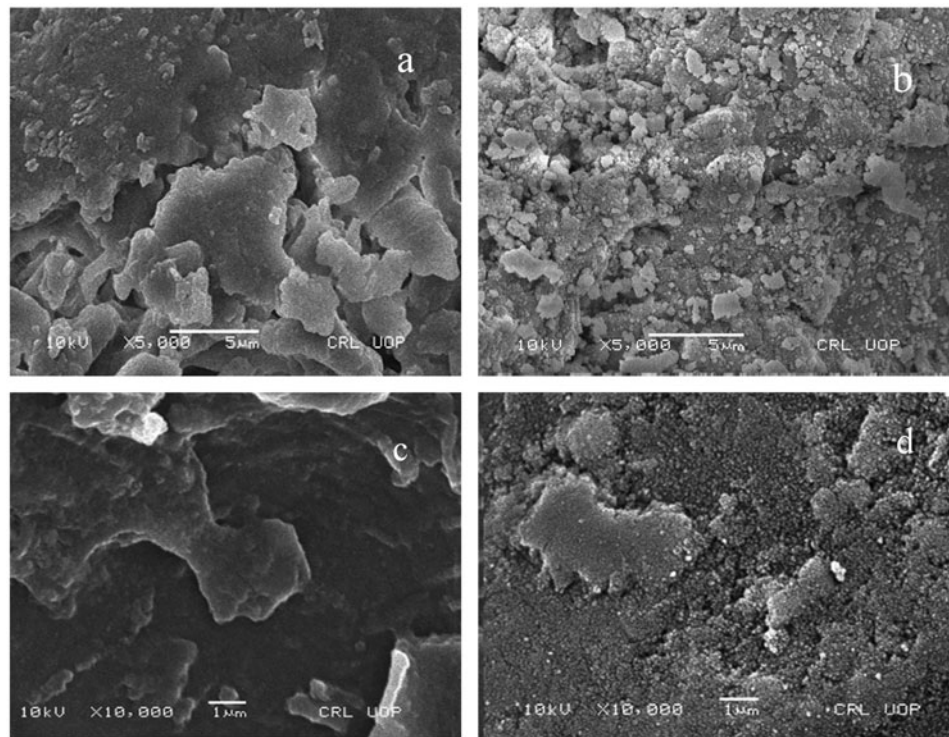


Fig. 1. SEM images of (a) UAS and (b) MIAS before MV2B adsorption, while (c) UAS and (d) MIAS after MV2B adsorption.

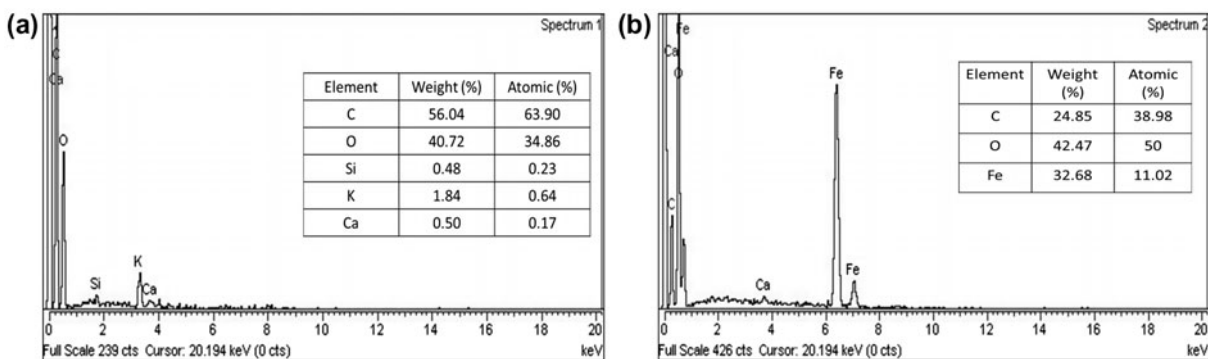


Fig. 2. EDX spectra of (a) UAS and (b) MIAS.

iron, oxygen, and carbon, while the other element present in the EDX spectra of UAS is completely missing in the EDX spectrum of MIAS. The high percentage of iron present in the EDX spectrum of MIAS reveals that the almond shell was successfully impregnated with magnetite (Fe_3O_4).

3.3. FT-IR study

The FT-IR analyses were performed in the range of $4,000\text{--}450\text{ cm}^{-1}$ in order to explore the surface characteristics of the adsorbents. Fig. 3 shows the FT-IR spectrum of UAS and MIAS. The spectrum shows a broadband at $3,400\text{ cm}^{-1}$, which is due to the presence of OH functional group. The peak appeared at $2,900\text{ cm}^{-1}$ is due to the aliphatic CH group. The bands appeared at $1,640$ and $1,380\text{ cm}^{-1}$ are due to stretching vibration of carbonyl group and C–H deformation vibration, respectively. The peak appeared at about $1,080\text{ cm}^{-1}$ reflects the stretch vibration of C–O. Fig. 3 also shows that the FT-IR spectrum of MIAS is similar with that of UAS except a peak (appeared at 578 cm^{-1}), which is assigned to Fe–O group.

3.4. Zeta potential of adsorbents before and after adsorption of Methyl Violet 2B dye

The adsorption of MV2B was more favorable at elevated pH, which is strongly supported by zero point charge analysis. At higher pH ($\text{pH} > \text{pH}_{\text{ZPC}}$), the surface of UAS and MIAS attains negative charge and the cationic dye (MV2B) is positively charged, due to which strong electrostatic force of attraction exists between dye and adsorbent. In contrast, at lower pH ($\text{pH} < \text{pH}_{\text{ZPC}}$), the surface of UAS and MIAS attains positive charge, which leads to decrease in dye uptake due to electrostatic repulsion between positively

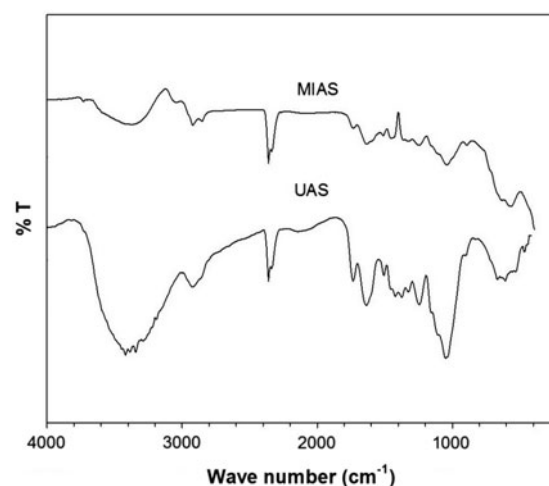


Fig. 3. FT-IR spectra of UAS MIAS.

charged adsorbent surface and cationic dye. The pH_{ZPC} of both adsorbents was also measured after the adsorption of MV2B showed that the MV2B shifted pH_{ZPC} curve of both adsorbents in positive direction. It can be concluded that the MV2B adsorbed specifically to the surface of UAS and MIAS, because during the specific adsorption positive molecules of dye are transferred to the surface of UAS and MIAS, which decreases the negative or increase the positive charge of both adsorbents.

3.5. Effect of pH in the removal of MV2B

Solution pH plays an important role during the removal of dyes from aqueous solution by adsorbents because it affects the adsorbent surface and dye structure [25]. Fig. 4 shows the percentage removal of MV2B at different pH (pH range 2–12) at constant conditions such as temperature (28°C), initial dye concentration

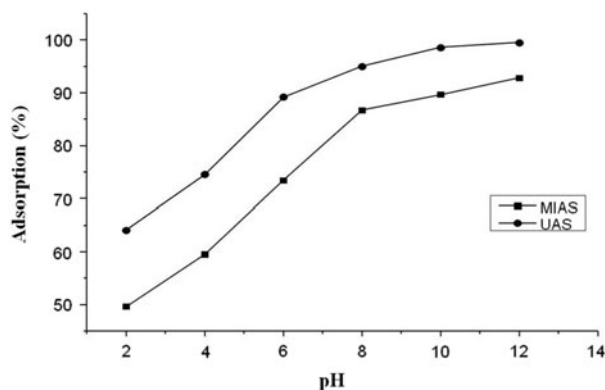


Fig. 4. Effect of pH on the adsorption of MV2B onto UAS and MIAS (temperature: 28°C; initial dye concentration: 40 mg/L; and adsorbent dose: 0.05 g).

(40 mg/L of 30 mL), and adsorbent dose (0.05 g). The results showed that percent removal of dye increases with increasing the solution pH. In acidic medium, the MV2B adsorption was unfavorable because adsorbent surface is positively charged, which repelled the cationic molecules of MV2B dye [25]. Moreover, in acidic medium, the solutions contains, abundant H^+ ions, which competed with the cationic molecules of the MV2B dye for the binding to the active sites of the adsorbents, and thereby inhibiting the dye adsorption from solution to the surface of adsorbent [26]. In basic medium, the adsorbent surface may become negatively charged which enhance the adsorption of cationic dye due to electrostatic attraction [26,27].

3.6. Effect of contact time

The adsorption of MV2B from aqueous solutions onto UAS and MIAS was carried out at different time intervals in order to find out the equilibrium adsorption time. Fig. 5 shows that the adsorption of MV2B from aqueous solution onto UAS and MIAS increases with increasing contact time and then almost become constant after 80 min. The result also presented that the MIAS adsorbed more quantity of MV2B from aqueous medium as compared to UAS.

3.7. Adsorption kinetics

In order to find the mechanism for the adsorption of MV2B onto UAS and MIAS, kinetic data were checked through pseudo-first-order kinetic, pseudo-second-order kinetic, and the intraparticle diffusion model.

The Lagergren proposed pseudo-first-order kinetic model is given as [28]:

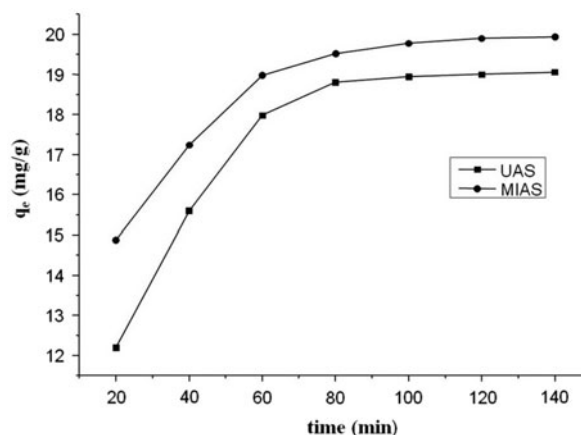


Fig. 5. Effect of contact time on the adsorption of MV2B onto UAS and MIAS (initial dye concentration: 40 mg/L; pH: 8; temperature: 25°C; and adsorbent dose: 0.05 g).

$$\text{Log}(q_e - q_t) = \text{Log} q_e - K_1 t / 2.303 \quad (3)$$

where q_e and q_t are the concentration of dye adsorbed (mg/g) at equilibrium and at respective time, and k_1 is the rate constant of pseudo-first-order kinetic model and that can be calculated from the linear plot of $\text{Log}(q_e - q_t)$ vs. time.

The linear form of pseudo-second-order kinetic model is given as follows [29]:

$$\frac{t}{q_t} = \frac{1}{k_2 q_e^2} + \frac{1}{q_e} t \quad (4)$$

By plotting t/q_t vs. t give a straight line from which K_2 (mg/L) and q_e (mg/g) can be calculated.

The intraparticle diffusion model is given as follows [29]:

$$q_t = K_{id} t^{1/2} + C \quad (5)$$

In Eq. (5), q_t is the amount of dye adsorbed at the surface of adsorbent at respective time, K_{id} is the intraparticle diffusion rate constant, and C is the intercept, which explain the thickness of boundary layer, i.e. greater the C value, larger will be the effect of boundary layer. If the kinetic studied followed the intraparticle diffusion model, the graph of q_t vs. $t^{1/2}$ will be passed from origin [30]. The results of intraparticle diffusion model of both types of adsorbents consist of two different stages. The first stage represents the rapid adsorption of MV2B molecules on the adsorbent surface through boundary layer diffusion process, in which molecules of dye move from solutions to the surface of the adsorbent with very fast rate and tend

Table 1

Parameters of pseudo-first-order, pseudo-second-order, and intraparticle diffusion models

Adsorbents	Pseudo-first-order				Pseudo-second-order			Intraparticle diffusion model	
	q_e^{exp} (mg/g)	q_e (mg/g)	K_1 (min) ⁻²	R^2	q_e (mg/g)	K_2 (mg/g min)	R^2	K_{id} (mg/g min) ^{1/2}	C (mg/g)
UAS	19.06	12.6	4.7×10^{-2}	0.9886	20	1×10^{-2}	0.997	1st stage 1.771 2nd stage 0.107	4.27 17.83
MIAS	19.94	15.8	4.9×10^{-2}	0.9885	21.3	5.7×10^{-3}	0.999	1st stage 1.24 2nd stage 0.133	9.39 18.41

to cover the pores of the adsorbent surface. The second stage represents the establishment of the equilibrium stage. The intraparticle diffusion parameters were obtained from plot of q_t vs. $t^{1/2}$, and the results were given in Table 1. The results show that the value of C (given in Table 1) in case of intraparticle diffusion model indicated that the adsorption process was mostly controlled by boundary layer adsorption [31,32].

Pseudo-first-order, pseudo-second-order, and intraparticle diffusion model parameters are given in Table 1. From the regression coefficient value (R^2) of all the three models, it is found that the kinetic data do not follow pseudo-first-order and intraparticle diffusion model, but it is best fitted to pseudo-second-order kinetic model. Moreover, in pseudo-second-order kinetic model, calculated q_e value is also very close to experimental q_e value.

3.8. Effect of adsorbent dose

Adsorption of MV2B from aqueous solutions on to UAS and MIAS was carried out at different adsorbent dose ranged from 0.02 to 0.1 g. Figs. 6 and 7 showed that with increasing adsorbent dose, the adsorption capacity (mg/g) decreased from 24.34 to 5.5 mg/g for UAS and from 26.34 to 10 mg/g for MIAS, while the percentage adsorption was increases from 49.5 to 95% for UAS and from 57 to 99.97% for MIAS. The increase in percentage adsorption with increase in adsorbent dose may be due to the availability of larger active sites on the adsorbent surface for the fixed amount of dye [33].

3.9. Effect of initial dye concentration

Adsorption of MV2B onto UAS and MIAS was carried out at different initial dye concentration ranged from 20 to 120 mg/L, and other conditions such as time (120 min), pH (8), temperature (25°C), and

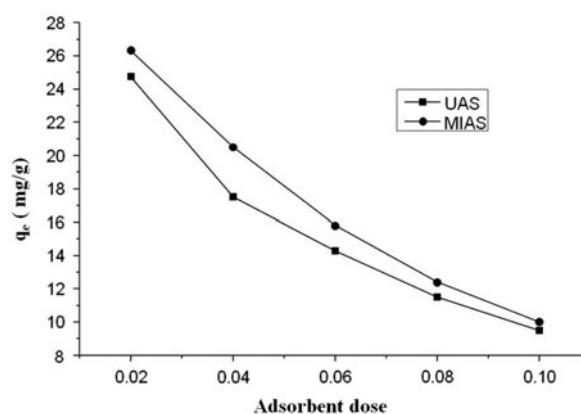


Fig. 6. Effect of adsorbent dose (mg/g) on the adsorption of MV2B onto UAS and MIAS (initial dye concentration: 40 mg/L; temperature: 25°C; pH: 8; and time: 120 min).

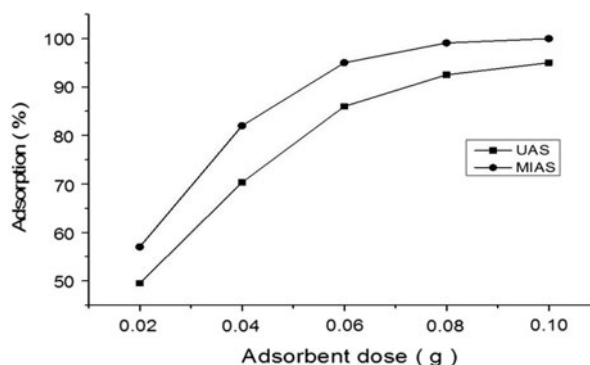


Fig. 7. Effect of adsorbent dose on the percentage adsorption of MV2B to UAS and MIAS (initial dye concentration: 40 mg/L; temperature: 25°C; pH: 8; and time: 120 min).

amount of adsorbent (0.05 g) were kept constant. Figs. 8 and 9 showed the adsorption in mg/g and in percentage. The results presented that the adsorption of MV2B decreases with increasing the initial dye

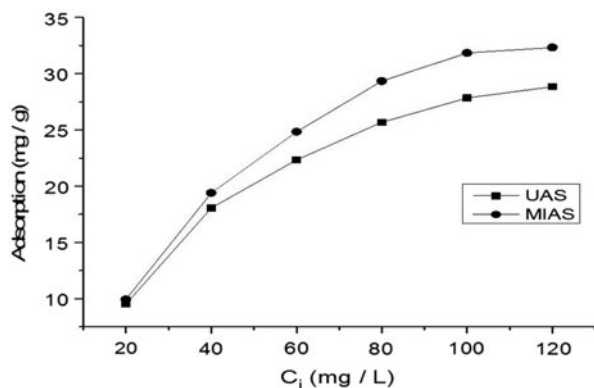


Fig. 8. Effect of initial dye concentration on the adsorption (mg/g) of MV2B to UAS and MIAS (adsorbent dose: 0.05 g; temperature: 25°C; pH: 8; and time: 120 min).

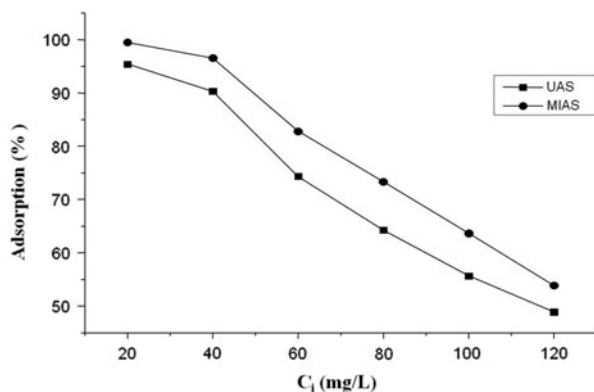


Fig. 9. Effect of initial dye concentration on the adsorption (percentage) of MV2B to UAS and MIAS (adsorbent dose: 0.05 g; temperature: 25°C; pH: 8; and time: 120 min).

concentration. It is due to at lower concentration of MV2B, the percent adsorption was high, which was due to availability of high adsorbent surface for the lower concentration of dye molecules, and then decreases with increasing the dye concentration due to saturation of the adsorbent sites with the dye mole-

cules. The adsorption of dye per unit mass of adsorbent was increased as increased the dye concentration, which might be contributed to decrease in resistance for dye molecules to adsorb from aqueous solutions to adsorbent surface [33].

3.10. Adsorption Isotherm

In this work, Langmuir and Freundlich adsorption isotherms were used in order to interpret the isotherm data of MV2B onto UAS and MIAS.

The Freundlich adsorption isotherm, used for heterogeneous surface, is given as follows [34,35]:

$$\ln q_e = \ln K_F + \frac{1}{n} \ln C_e \quad (6)$$

where q_e (mg/g) is the amount of dye adsorbed at equilibrium, C_e (mg/L) is the remaining concentration in solution, K_F (mg/g) (L/mg) and n are the constant which can be calculated from the slope and intercepts of linear plot of $\ln q_e$ vs. $\ln C_e$.

The linear form of Langmuir isotherm is given as follows [36,37]:

$$\frac{C_e}{q_e} = \frac{1}{Kq_{\max}} + \frac{C_e}{q_{\max}} \quad (7)$$

The parameters of Freundlich and Langmuir, which were obtained from both the linear plots, are given in Table 2. From the parameters of Freundlich and Langmuir adsorption isotherms, it can be concluded that the adsorption data are best fitted to Langmuir adsorption isotherm as compared to Freundlich adsorption isotherm.

3.11. Effect of temperature

Temperature has a pronounced effect on the adsorption of dyes onto adsorbent. Therefore, the adsorption studied was carried out at different temperature ranged from 30 to 60°C. Fig. 10 presented

Table 2
Parameters of Freundlich and Langmuir adsorption isotherm models

Adsorbents	Freundlich isotherm			Langmuir isotherm	
	K_F (L/mg)	n	R^2	K_L (L/mg)	R^2
MV2B Adsorption on UAS	10.71	3.9	0.9362	0.298	0.9968
MV2B Adsorption on MIAS	16.3	5.4	0.9414	0.63	0.9971

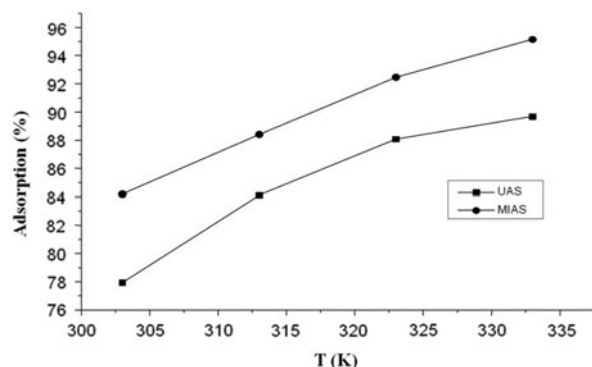


Fig. 10. Effect of temperature on the adsorption of MV2B onto UAS and MIAS.

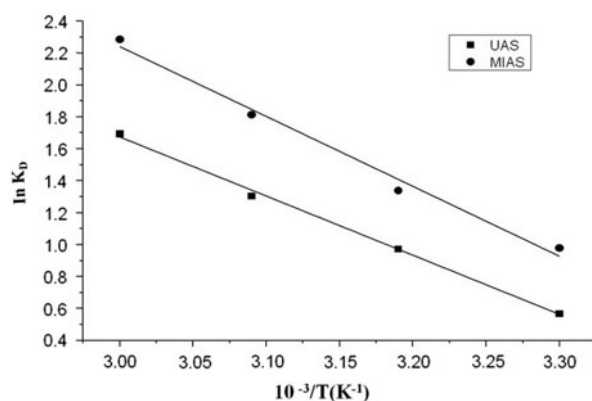


Fig. 11. The Van't Hoff plots for the adsorption of MV2B onto UAS and MIAS.

that the percent adsorption of MV2B increased from 77.9 to 89.6% onto UAS and from 84 to 95% onto MIAS with increase in temperature from 30 to 60°C. The adsorption capacity also increased from 23.4 to 26.9 mg/g for UAS and from 25.3 to 28.5 mg/g for MIAS with increase in temperature. The adsorption of MV2B onto UAS and MIAS increased with increase in

temperature, which was due to the widening of pores and some active sites formation on the surface of adsorbent due to bond cleavage with increase in temperature [38]. Moreover, the diffusion rate in the pore of adsorbent also increased with increase in temperature.

3.12. Thermodynamic parameters

The temperature effect on the adsorption of MV2B onto UAS and MIAS is explained further by thermodynamic parameters. Thermodynamic parameters, i.e. change in free energy (ΔG), change in enthalpy (ΔH), and change in entropy (ΔS), were investigated by the following equations [39]:

$$\Delta G = -RT \ln K_D \quad (8)$$

$$\ln K_D = \frac{\Delta S}{R} - \frac{\Delta H}{RT} \quad (9)$$

$$\ln K_D = \frac{q_e}{C_e}$$

where K_D is the distribution coefficient, R is the ideal gas constant (8.314 kJ/mol), and T is the absolute temperature in kelvin. $\ln K_D$ were plotted vs. $1/T$ as given in Fig. 11. The value of ΔH and ΔG was calculated from the slopes and intercepts of linear plot of $\ln K_D$ vs. $1/T$. While the value of ΔG was calculated through Eq. (8). The value of ΔG , ΔH , and ΔS is given in Table 3. The value of ΔG is negative, which indicates that the adsorption is spontaneous in nature [40]. The value of ΔS is positive, which suggests that the MV2B molecule adsorbed randomly on the surface of adsorbent, while the positive value of ΔH conforms the thermodynamic nature of the present adsorption studied [41].

Table 3
Thermodynamic parameters for the adsorption of MV2B on UAS and MIAS

Samples	ΔH (kJ/mol)	ΔS (kJ/mol K)	$-\Delta G$ (kJ/mol)			
			303 K	313 K	323 K	333 K
MV2B on UAS	30.8	106.23	1.432	2.534	3.506	4.689
MV2B on MIAS	36.34	127.62	2.469	3.485	4.872	6.327

4. Conclusion

In this study, the adsorptive removal of MV2B from wastewater onto UAS and MIAS was investigated. From the experimental results, it was concluded that the adsorption capacity of MIAS for MV2B was high than UAS. The high adsorption capacity of MIAS over UAS was due to its more porous and rough surface. The high adsorption capacity of MIAS can also be contributed to better interaction of magnetite nanoparticles with MV2B molecules. The equilibrium isotherm data were analyzed by Freundlich and Langmuir adsorption isotherm models, which were best fitted to Langmuir adsorption isotherm model. The kinetic studies were checked by theoretical kinetic models such as pseudo-first-order, pseudo-second-order, and intraparticle diffusion models, which were followed pseudo-second-order kinetic model.

References

- [1] S.-M. Lam, J.-C. Sin, A.Z. Abdullah, A.R. Mohamed, Degradation of wastewaters containing organic dyes photocatalysed by zinc oxide: A review, *Desalin. Water Treat.* 41 (2012) 131–169.
- [2] M. Ghaedi, H. Hossainian, M. Montazerzohori, A. Shokrollahi, F. Shojai pour, M. Soylak, M.K. Purkait, A novel acorn based adsorbent for the removal of brilliant green, *Desalination* 281 (2011) 226–233.
- [3] V.S. Mane, P.V.V. Babu, Studies on the adsorption of brilliant green dye from aqueous solution onto low-cost NaOH treated saw dust, *Desalination* 273 (2011) 321–329.
- [4] B.K. Nandi, A. Goswami, M.K. Purkait, Removal of cationic dyes from aqueous solutions by kaolin: Kinetic and equilibrium studies, *Appl. Clay Sci.* 42 (2009) 583–590.
- [5] J.S. Wu, C.H. Liu, K.H. Chu, S.Y. Suen, Removal of cationic dye methyl violet 2B from water by cation exchange membranes, *J. Membr. Sci.* 309 (2008) 239–245.
- [6] C.G. Kumar, P. Mongolla, J. Joseph, V.U.M. Sarma, Decolourization and biodegradation of triphenylmethane dye, brilliant green, by *Aspergillus* sp., Isolated from Ladakh, India *Process Biochem.* 47 (2012) 1388–1394.
- [7] F.K. Bangash, A. Manaf, Kinetics of removal of dye (Basic Blue 3) from aqueous solutions by activated charcoal prepared from the wood of *Brausonia papyrifera* (Paper Mulberry), *J. Chem. Soc. Pak.* 26 (2004) 111–115.
- [8] P. Sharma, H. Kaur, M. Sharma, V. Sahore, A review on applicability of naturally available adsorbents for the removal of hazardous dyes from aqueous waste, *Environ. Monit. Assess.* 183 (2011) 151–195.
- [9] Y. Khambhaty, K. Mody, S. Basha, Efficient removal of brilliant blue G (BBG) from aqueous solutions by marine *Aspergillus wentii*: Kinetics, equilibrium and process design, *Ecol. Eng.* 41 (2012) 74–83.
- [10] V.S. Mane, I.D. Mall, V.C. Srivastava, Kinetic and equilibrium isotherm studies for the adsorptive removal of brilliant green dye from aqueous solution by rice husk ash, *J. Environ. Manage.* 84 (2007) 390–400.
- [11] R. Dhodapkar, N.N. Rao, S.P. Pande, S.N. Kaul, Removal of basic dyes from aqueous medium using a novel polymer: Jalshakti, *Bioresour. Technol.* 97 (2006) 877–885.
- [12] M.S. Tanyildizi, Modeling of adsorption isotherms and kinetics of reactive dye from aqueous solution by peanut hull, *Chem. Eng. J.* 168 (2011) 1234–1240.
- [13] Y. Safa, H.N. Bhatti, Kinetic and thermodynamic modeling for the removal of Direct Red-31 and Direct Orange-26 dyes from aqueous solutions by rice husk, *Desalination* 272 (2011) 313–322.
- [14] G.H. Sonawane, V.S. Shrivastava, Kinetics of decolourization of malachite green from aqueous medium by maize cob (*Zea mays*): An agricultural solid waste, *Desalination* 247 (2009) 430–441.
- [15] B. Samiey, A.R. Toosi, Adsorption of malachite green on silica gel: Effects of NaCl, pH and 2-propanol, *J. Hazard. Mater.* 184 (2010) 739–745.
- [16] A. Adak, M. Bandyopadhyay, A. Pal, Removal of crystal violet dye from wastewater by surfactant-modified alumina, *Sep. Purif. Technol.* 44 (2005) 139–144.
- [17] F.D. Doulati Ardejani, K. Badii, N.Y. Limaee, S.Z. Shafaei, A.R. Mirhabibi, Adsorption of Direct Red 80 dye from aqueous solution onto almond shells: Effect of pH, initial concentration and shell type, *J. Hazard. Mater.* 151 (2008) 730–737.
- [18] H.B. Senturk, D. Ozdes, C. Duran, Biosorption of Rhodamine 6G from aqueous solutions onto almond shell (*Prunus dulcis*) as a low cost biosorbent, *Desalination* 252 (2010) 81–87.
- [19] T. Madrakian, A. Afkhami, M. Ahmadi, Adsorption and kinetic studies of seven different organic dyes onto magnetite nanoparticles loaded tea waste and removal of them from wastewater samples, *Spectrochim. Acta, Part A.* 99 (2012) 102–109.
- [20] M. Ishaq, K. Saeed, M. Shakirullah, I. Ahamad, S. Sultan, Removal of Murexide from aqueous solution using pomegranate bark as an adsorbent, *J. Chem. Soc. Pak.* 34 (2012) 1498–1501.
- [21] H. Dolas, O. Sahin, C. Saka, H. Demir, A new method on producing high surface area activated carbon: The effect of salt on the surface area and the pore size distribution of activated carbon prepared from pistachio shell, *Chem. Eng. J.* 166 (2011) 191–197.
- [22] C. Saka, BET, TG–DTG, FT-IR, SEM, iodine number analysis and preparation of activated carbon from acorn shell by chemical activation with ZnCl₂, *J. Anal. Appl. Pyrolysis* 95 (2012) 21–24.
- [23] M. Özdemir, T. Bolgaz, C. Saka, Ö. Şahin, Preparation and characterization of activated carbon from cotton stalks in a two-stage process, *J. Anal. Appl. Pyrolysis* 92 (2011) 171–175.
- [24] V.K. Garg, R. Gupta, A.B. Yadav, R. Kumar, Dye removal from aqueous solution by adsorption on treated sawdust, *Bioresour. Technol.* 89 (2003) 121–124.
- [25] M. Fang, X.M. Cai, D.Z. Wei, T.Y. Xiao, F. Ning, W.F. Hong, Removal of rhodamine B using iron pillared bentonite, *J. Hazard. Mater.* 155 (2011) 602–609.

- [26] B.H. Hameed, E.I. Khaiary, Removal of basic dye from aqueous medium using a novel agriculture seed hull, *J. Hazard. Mater.* 155 (2008) 602–609.
- [27] L. Wang, J. Li, Y. Wang, L. Zhao, Q. Jiang, Adsorption capability for Congo red on nanocrystalline MFe_2O_4 ($M=Mn, Fe, Co, Ni$) spinel ferrites, *Chem. Eng. J.* 181–182 (2012) 72–79.
- [28] B.H. Hameed, Equilibrium and kinetic studies of methyl violet sorption by agricultural waste, *J. Hazard. Mater.* 154 (2008) 204–212.
- [29] D. Kaušpėdienė, E. Kazlauskienė, A. Gefenienė, R. Binkienė, Comparison of the efficiency of activated carbon and neutral polymeric adsorbent in removal of chromium complex dye from aqueous solutions, *J. Hazard. Mater.* 179 (2010) 933–939.
- [30] N. Kannan, M.M. Sundaram, Kinetics and mechanism of removal of methylene blue by adsorption on various carbons—A comparative study, *Dyes Pigm.* 51 (2001) 25–40.
- [31] D. Ozdes, C. Duran, H.B. Senturk, H. Avan, B. Bicer, Kinetics, thermodynamics, and equilibrium evaluation of adsorptive removal of methylene blue onto natural illitic clay mineral, *Desalin. Water Treat.* 52 (2014) 208–218.
- [32] H. Serencam, D. Ozdes, C. Duran, H.B. Senturk, Assessment of kinetics, thermodynamics, and equilibrium parameters of Cu(II) adsorption onto *Rosa canina* seeds, *Desalin. Water Treat.* 52 (2014) 3226–3236.
- [33] S. Yusra, B.N. Haq, kinetic and thermodynamic modeling for the removal of Direct Red-31 and Direct Orange -26 from aqueous solutions by rice husk, *Desalination* 272 (2011) 313–322.
- [34] L. Qian, S. Qinyan, S. Yuan, G. Baoyu, Equilibrium and two-stage batch absorber design for reactive or disperse dye removal to minimize adsorbent amount, *Bioresour. Technol.* 102 (2011) 5290–5296.
- [35] H.M.F. Freundlich, Uber die adsorption in lösungen, *Z. Phys. Chem.* 57 (1906) 385–470.
- [36] I. Langmuir, The adsorption of gases on plane surfaces of glass, mica and platinum, *J. Am. Chem. Soc.* 40 (1918) 1361–1403.
- [37] N.R. Aleksandra, V.J. Sava, A.G. Dtusan, Characterization of chitosan montmorillonite membrane as adsorbent for Bezactiv Orange V-3R dyes, *J. Hazard. Mater.* 209 (2012) 256–263.
- [38] F. Wu, R. Tseng, R. Juang, Pore structure and adsorption performance of the activated carbons prepared from plum kernels, *J. Hazard. Mater.* 69 (1999) 287–302.
- [39] E. Eren, B. Afsin, Investigation of a basic dye adsorption from aqueous solution onto raw and pre-treated bentonite surfaces, *Dyes Pigm.* 76 (2008) 220–225.
- [40] M. Arami, N.Y. Limaee, N.M. Mahmoodi, N.S. Tabrizi, Equilibrium and kinetics studies for the adsorption of direct and acid dyes from aqueous solution by soy meal hull, *J. Hazard. Mater.* 135 (2006) 171–179.
- [41] I. Uzun, Kinetics of the adsorption of reactive dyes by chitosan, *Dyes Pigm.* 70 (2006) 76–83.